Contents list available at CBIORE journal website

International Journal of Renewable Energy Development

Journal homepage: https://ijred.cbiore.id

Research Article

Simultaneous effect of precursor sources and concentration on structural, morphological and optical properties of ZnO nanostructured thin films for photovoltaic applications

Ognanmi Ako[a,b], Mazabalo Baneto[a,b*], Muthusamy Senthilkumar[c], Muthiah Haris[c], Alphonse Déssoudji Gboglo[a,b], Komlan Segbéya Gadedjisso-Tossou[a,d], Ayayi Claude Ahyi[e,f], Katawoura Beltako[a,d], Komi Apélété Amou[a,b]

[a] *Regional Center of Excellence for Electricity Management (CERME), University of Lomé, 01BP 1515, Lomé, Togo*

[b] *Laboratory on Solar Energy, Department of Physics, Faculty of Sciences, University of Lomé, 01BP 1515, Lomé, Togo*

[c] *School of Arts and Natural Sciences, Joy University, Raja Nagar, Vadakangulam, Near Kanyakumari, Tirunelveli Dist.-627116, Tamil Nadu, India*

[d] *Physics of Semiconductor Materials and Components Laboratory, Department of Physics, Faculty of Sciences, University of Lomé, 01BP 1515, Lomé, Togo*

[e] *Physics Department, Auburn University, Auburn, AL 36849, United State of America (USA)*

[f] *National Coalition of Independent Scholars, United State of America (USA)*

Abstract. The collection and transport of charges at the electrodes are the main factors limiting the efficiency of organic solar cells. Zinc oxide (ZnO) in nanostructured form helps to overcome this problem by introducing a ZnO buffer layer between the photoanode and the donor material. To achieve this, the ZnO thin film must exhibit good crystallinity, along with good electrical conductivity and high optical transparency in the visible range. The aim of this work is to investigate the effect of precursor sources and precursor concentrations on the structural, morphological, and optical properties of ZnO thin films. Three different precursor sources have been used: zinc acetate, zinc chloride and zinc nitrate. In each deposition solution, the precursor concentration varied from 0.1 M to 0.3 M. The ZnO films were deposited on glass substrates and all the films were annealed at 400°C for 3 hours. The structural, morphological and optical properties of deposited films were investigated using X-ray diffraction (XRD), scanning electron microscopy (SEM), and UV-visible spectroscopy respectively. XRD results showed that, regardless of the precursor source, all the ZnO films are polycrystalline with a hexagonal wurtzite structure. ZnO films obtained from acetate and nitrate sources crystallize preferentially along (002) and the peak intensity increases as the precursor concentration increases. SEM images showed that all the ZnO films are homogeneous, but films deposited from zinc acetate and zinc nitrate looked more compact and smoother than those obtained with zinc chloride which looked porous. UV-visible spectroscopy results revealed that the films transmittance depends both on precursor source and concentration. ZnO thin films deposited from zinc acetate at 0.3M concentration exhibit the best transmittance of 95% due to their smooth and uniform surfaces. The band gap of ZnO obtained from the zinc acetate precursor decreases with increasing solution concentration. It is found to be 3.29 eV, 3.26 eV, and 3.22 eV for concentrations of 0.1 M, 0.2 M, and 0.3 M, respectively. It therefore appears that ZnO films obtained from zinc acetate can be used as an electron transport layer for solar cells as they exhibit the best crystallinity and the highest transmittance.

Keywords: zinc oxide, nanostructure, precursor concentration, precursor source, spray pyrolysis

Received: 6th January 2025; Revised: 19th Feb 2025; Accepted: 29th March 2025; Available online: 3rd April 2025

1. Introduction

In recent years, climate change, energy and fuel sourcing and cost have been one of the world's major concerns. Thus, there is a critical need for sustainable energy resources. Photovoltaic technology has emerged as one of the best alternatives to fossil fuels (Ekmekci *et al.*, 2019). Today, over 95% of the photovoltaic cell market is dominated by silicon solar cells. However, silicon solar cell manufacturing technologies are expensive, and the product is out of reach of the public in most countries. For this reason, new solar cell technologies such as organic solar cells are being studied as alternatives to silicon-based solar cells. These studies are being carried out using new organic materials. They generally consist of a photo-active layer sandwiched between two electrodes. The first organic solar cell was discovered in 1959 by H. Kallmann (Hatem *et al.*, 2023), who reported a photovoltaic effect when he placed an anthracene single crystal between two silver electrodes. However, the performance obtained with such a structure was very low. Since then, significant progress has been made in this field to improve the efficiency of organic solar cells. Considerable efforts have been devoted to studying solution-based photovoltaic systems with both organic and inorganic compositions. These systems explore a wide variety of materials, including polymers (J. Chen *et al.*, 2015; Fu *et al.*, 2021; He *et al.*, 2015; Sun *et al.*, 2018), small molecules (H. Chen

---

[*] Corresponding author
Email: mazbaneto@gmail.com (M. Baneto)

https://doi.org/10.61435/ijred.2025.61069

et al., 2019; Zhou *et al.*, 2019), quantum dots, and perovskite photovoltaic cells. Polymer solar cells (PSC) began as single active layers, followed by donor-acceptor bilayers, then planar heterojunctions. The bulk heterojunction breakthrough significantly improved the charge separation mechanism (Abdulrazzaq *et al.*, 2013; Krebs, 2009; G. Li *et al.*, 2012; Y. Lin *et al.*, 2019). The bulk heterojunction architecture was introduced to address the issue of limited exciton diffusion length, which was previously a challenge in organic solar cells (Halls *et al.*, 1995; G. Yu *et al.*, 1995). Organic solar cells often contain elements such as a transparent conductive anode, indium or fluorine tin oxide (ITO or FTO), a Hole Transport Layer (HTL) made of poly(3,4-ethylenedioxythiophene)/poly (styrene sulfonate) acid (PEDOT: PSS), a low-work-function metallic cathode such as aluminum (Al) or calcium (Ca), and a photoactive layer composed of a blend of a bulk heterojunction conjugated polymer and a fullerene derivative. The use of low work function metals like Al or Ca in the cathode, which are sensitive to atmospheric oxygen and water (Jørgensen *et al.*, 2008; Krebs *et al.*, 2007; Salsberg *et al.*, 2019) limits device long-term stability. This must be overcome through encapsulation to prevent degradation due to moisture and oxygen (Osorio *et al.*, 2017). Additionally, the high acidity, corrosive properties, and hygroscopic nature of PEDOT:PSS further reduce device lifetime (De Jong *et al.*, 2000; Wong *et al.*, 2002), as degradation occurs at ITO/PEDOT:PSS interface. To address this latter issue and prevent corrosion between ITO and PEDOT: PSS, researchers have developed inverted polymer solar cells (iPSC), in which the Electron Transport Layer (ETL) is in contact with the ITO instead. In this approach, the iPSC achieve better performance (Balderrama *et al.*, 2018; He *et al.*, 2012). In iPSCs, the type of electron transport layer is one of the important factors in limiting device performance. The commonly used ETLs in iPSCs include titanium dioxide (TiO_2), zinc oxide (ZnO), cesium carbonate (Cs_2CO_3), and poly [(9,9- bis(3-(N,N-dimethylamino) propyl) - 2,7-fluorene) – alt - 2,7 - (9,9 dioctylfluorene)] (PFN) (Li *et al.*, 2020; Osorio *et al.*, 2017).

ZnO thin films have been considered as one of the most promising oxide materials due to their high chemical stability and electrical properties. It is often regarded as an ideal material for roll-to-roll manufacturing, particularly when applied to flexible substrates (Cho *et al.*, 2019). Various methods, such as the sol-gel method (Arifin *et al.*, 2024; Foo *et al.*, 2014),spin coating (Arifin *et al.*, 2024; Mishra *et al.*, 2024), hydrothermal growth (Akir *et al.*, 2017; Podlogar *et al.*, 2012; Shrisha *et al.*, 2016), vapor-phase deposition (Zhang *et al.*, 2013), have been explored for preparing various ZnO nanostructures. However, few studies have been conducted on iPSCs using ZnO ETLs films obtained from spray pyrolysis technique (Moustafa *et al.*, 2021). This technique offers numerous advantages such as its cost-effectiveness, ease of use, ability to produce uniform coatings over large areas, control over film characteristics, low processing temperatures, and reproducibility (Dakhsi *et al.*, 2014; Ravichandran *et al.*, 2016). In this work, ZnO thin films were synthesized using the spray pyrolysis technique. The effects of the concentration of three different precursors (zinc acetate, zinc chloride and zinc nitrate) on the structural, morphological and optical properties of ZnO have been studied.

2. Experimental details and characterization

2.1 Materials and reagents

Microscope glass slides were used as substrates to deposit different ZnO thin films. All the chemicals, such as zinc acetate dihydrate $(CH_3COO)_2Zn, 2H_2O)$, zinc chloride $(ZnCl_2)$ and zinc nitrate hexahydrate $(Zn(NO_3)_2.6H_2O)$, were purchased from Sigma-Aldrich. All analytical grade (AR) chemicals (Ethanol (C_2H_6O), acetone $[(CH_3)_2CO]$, nitric acid (HNO_3) and distilled water) have purity above 99 % and were utilized without further treatment. A mixed solvent composed of distilled water and ethanol in 2:3 ratio was used. This alcoholic solvent was chosen because its surface tension and viscosity have been shown to be low (Kärber *et al.*, 2011). This results in a small droplet size, enabling homogeneous distribution on the substrate. In addition, the high volatility of the alcoholic solvent is likely to reduce the cooling rate of the substrate.

2.2 Substrate cleaning

Glass substrates with dimensions of 2.5 cm × 2.0 cm were used. First, the substrates were immersed in an aqueous solution of nitric acid for a few minutes to remove contamination such as airborne dust. Next, the substrates were rinsed in distilled water then successively cleaned using an ultrasonic bath in, acetone, ethanol, and distilled water for 15 minutes each to eliminate all organic and inorganic contaminants. Finally, the substrates were dried under a stream of hot air using a consumer grade hair dryer.

2.3 Formation of ZnO nanostructured thin films

The ZnO nanorods were deposited on glass substrates at 350°C using a spray pyrolysis deposition system (HOLMARC, HO-TH-64). To study the effect of the precursor solution and its concentration, three separate zinc precursor solutions were prepared from zinc acetate dihydrate, zinc chloride and zinc nitrate hexahydrate, respectively. For each solution, a weighted quantity of precursor was dissolved in the 2:3 deionized water and ethanol mixture. A few drops of hydrochloric acid were added to the solutions to avoid the precipitation of zinc hydroxide. After 15 minutes of magnetic stirring, the solution became clear and transparent, ready to be deposited using the spray pyrolysis device. The concentration of each precursor solution was varied from 0.1 M to 0.3 M with a step of 0.1 M. A volume of 20 mL of solution was sprayed onto the glass substrate initially heated to 350°C. The same procedure was repeated for each precursor. After deposition, the films were annealed in air at a temperature of 400°C for 3 hours. The chemical reactions that occur during the anneals are described below.

2.3.1 Case of zinc acetate precursor

According to reported works (C.-C. Lin *et al.*, 2009), the formation of ZnO nanostructures using zinc acetate precursor and a mixed solvent (water and ethanol) results in several pyrolytic reactions. Initially, when the zinc acetate solution is sprayed as an aerosol onto the substrate, a dehydration reaction occurs transforming hydrated zinc acetate into anhydrous zinc acetate (eq.1). Then, the sublimation of the latter leads to basic zinc acetate as described by equation (2). Finally, a pyrolysis and decarboxylation reaction (eq.3) of basic zinc acetate results in the formation of ZnO.

$$Zn(CH_3-COO)_2,\ 2H_2O \xrightarrow{heat} Zn(CH_3-COO)_2 + 2H_2O \qquad (1)$$

$$4Zn(CH_3-COO)_2 + 2H_2O \xrightarrow{heat} Zn_4O(CH_3-COO)_6 + 2CH_3-COOH^{\uparrow} \qquad (2)$$

$$Zn_4O(CH_3-COO)_6 \xrightarrow{heat} 4ZnO + 3CH_3-COCH_3^{\uparrow} + 3CO_2^{\uparrow} \qquad (3)$$

In summary, the production of ZnO involves a series of pyrolytic decomposition reactions resulting in the production of three volatile molecules such as acetone, acetic acid, and carbon dioxide (eq.4), while zinc ions react with oxygen from water to form the corresponding oxide (eq.5) (Arca *et al.*, 2009).

$$Zn(CH_3-COO)_2\,,\ 2H_2O \xrightarrow{heat} ZnO\,, CH_3 - COCH_3^{\uparrow}, CH_3-COOH^{\uparrow}, CO_2^{\uparrow} \quad (4)$$

$$Zn^{2+} + O^{2-} \longrightarrow ZnO_{(solide)} \quad (5)$$

2.3.2 Case of zinc chloride precursor

Zinc oxide nanostructures are obtained by dissolving zinc chloride precursor in deionized water and ethanol in a ratio of 2:3. Although it is soluble in this mixture, Raman studies have shown that $ZnCl_2$ exists in the solvated state complex ($ZnO(H_2O)_6^{++}$ and $ZnCl_4(H_2O)_2^{-}$) instead of Zn^{2+}et Cl^{-}ions (Irish *et al.*, 1963) equation (6). The pyrolytic decomposition of hydrated zinc chloride on the heated substrate in presence of water following the reaction ($ZnCl_2 + H_2O \rightarrow ZnO + 2HCl$) (Mani *et al.*, 2014) is not the only one. Other reactions involving the formation of ZnO are also at play. When the zinc complexes in solution are sprayed onto the heated substrate, they form $ZnCl_2(H_2O)_4$ according to equation (7) (Thankalekshmi *et al.*, 2012). Then the latter, through an immediate thermal decomposition reaction, produces zinc hydroxychloride $Zn(OH)Cl$ (eq. 8). Finally, ZnO thin films are obtained by hydrolysis of zinc hydroxychloride, which may be partial or total (eq.9) (Kozawa *et al.*, 2011). The main chemical reactions describing the growth of ZnO NRs are as follows:

$$ZnCl_2 + 8H_2O \xrightarrow{stirring} ZnO(H_2O)_{6(solution)}^{++} + ZnCl_4(H_2O)_{2(solution)}^{-} \quad (6)$$

$$ZnO(H_2O)_{6(solution)}^{++} + ZnCl_4(H_2O)_{2(solution}^{-} \xrightarrow{crystallization} 2ZnCl_2(H_2O)_4 \quad (7)$$

$$2ZnCl_2(H_2O) \xrightarrow{decomposition} Zn(OH)Cl + 2HCl^{\uparrow} + 6H_2O^{\uparrow} \quad (8)$$

$$Zn(OH)Cl \xrightarrow{hydrolyse} 2ZnO_{(film)} + 2HCl^{\uparrow} \quad (9)$$

2.3.3 Case of zinc nitrate precursor

The thermal decomposition of $Zn(NO_3)_2.6H_2O$ leads to the formation of nitrogen oxides according to the equation (10), (Maneva *et al.*, 1989).

$$(Zn(NO_3)_2.6H_2O \xrightarrow{heat} ZnO + NO_2 + NO + O_2 + 6H_2O \quad (10)$$

2.4 Characterization of ZnO nanostructured thin films

To study the properties of the elaborated samples, various characterization techniques were used. The X-ray diffractometer model EMPYREAN, using Cu-Kα wavelength (λ=1.5406 Å), was used to identify the phases present in the samples and their crystalline structure. The surface morphology was characterized using ZEISS-EVO 18 scanning electron microscopy operating at an accelerating voltage of 15 kV. The detection of the presence of functional groups and bonds was carried out using Fourier-transform infrared spectroscopy (Perkin-Elmer Spectrum 3). UV-visible spectrophotometry (JASCO V-670 Model) was used to measure the optical transmittance of the elaborated thin films.

3. Results and discussion

3.1 Structural properties

Figure 1 shows the XRD spectra of ZnO thin films grown on glass substrates at 350°C, using zinc acetate (Fig. 1a), zinc chloride (Fig.1b) and zinc nitrate (Fig.1c) as precursors with different concentrations. It can be seen from the XRD spectra that precursor sources and precursor concentrations influence the ZnO thin films growth. The ZnO thin films obtained with 0.1 M grow randomly. However, by increasing the precursor concentration, films start to grow preferentially along the (002) axis. Furthermore, the films obtained from zinc chloride and zinc nitrate (Fig.1b and Fig.1c, respectively) grow also preferentially along the (002) axis as the precursor concentration increases. However, in the case of zinc chloride, the films start to grow randomly beyond 0.2 *M, indicating* the deterioration of the film's crystallinity. This phenomenon can be attributed to several factors: i) solutions with higher concentrations of zinc chloride tend to have higher viscosity and surface tension compared to those with lower concentrations or other precursors like zinc acetate. This increased viscosity can hinder the uniform spreading of droplets on the substrate surface, leading to a less uniform film

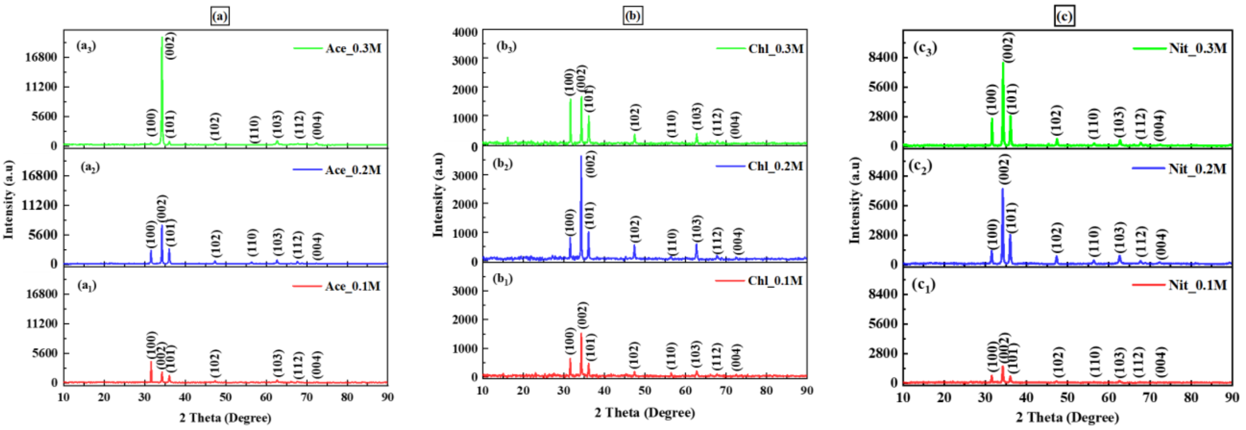

Fig. 1. XRD patterns of ZnO thin films using different precursors: (a) zinc acetate, (b) zinc chloride and (c) zinc nitrate, with varying different precursors: (a1, b1, c1) for 0.1M (a2, b2, c2) for 0.2M and (a3, b3, c3) for 0.3M.

Table 1
Texture coefficient of ZnO thin films along the dominant peaks (100), (002) and (101) for different concentration values using (a) zinc acetate, (b) zinc chloride and (c) zinc nitrate as precursors.

(a): zinc acetate			
Precursors concentration	$T_{C(hkl)}$		
	(100)	(002)	(101)
0.1M	1.62	1.14	0.34
0.2M	0.56	2.07	0.36
0.3M	0.05	2.94	0.08

(b): zinc chloride			
Precursors concentration	$T_{C(hkl)}$		
	(100)	(002)	(101)
0.1M	0.66	2.05	0.28
0.2M	0.39	2.32	0.28
0.3M	1.09	2.27	0.59

(c): zinc nitrate			
Precursors concentration	$T_{C(hkl)}$		
	(100)	(002)	(101)
0.1M	0.65	2.00	0.33
0.2M	0.31	2.27	0.39
0.3M	0.54	2.11	0.33

morphology (Al-Rasheedi *et al.*, 2022a); ii) higher viscosity solutions may result in larger droplets that do not spread as evenly, contributing to a more random or rough surface pattern (Lehraki *et al.*, 2012).

It is reported that, using spray pyrolysis technique, ZnO usually grows along the (002) orientation due to the low surface free energy of the (002) plane (Morinaga *et al.*, 1997).To confirm the degree of preferential orientation of crystallites along the (002) axis, the texture coefficient $T_{C(hkl)}$ for each peak was calculated using equation (11):

$$T_{C(hkl)} = \frac{\left[\frac{I_{(hkl)}}{I_{r(hkl)}}\right]}{\frac{1}{n}\left[\sum_n \left(\frac{I_{(hkl)}}{I_{r(hkl)}}\right)\right]} \tag{11}$$

where $T_{C(hkl)}$ is the texture coefficient, $I_{(hkl)}$ are the XRD intensities obtained from the thin films and n the number of diffraction peaks considered. $I_{r(hkl)}$ is the intensity of the XRD reference (JCPDS file 36-1451) of randomly oriented grains. The obtained $T_{C(hkl)}$ are reported in table 1. If $T_{C(hkl)} \simeq 1$ for all hkl planes considered, then the films have a randomly oriented crystallite. While $T_{C(hkl)}$ values greater than 1, indicate an abundance of grains in the given (hkl) direction. Values $0 < T_{C(hkl)} < 1$, indicate the absence of grains oriented in that direction. In Table 1, for samples obtained from acetate precursors, the texture coefficient along (002) peak increases from 1.14 to 2.94 as the solution concentration increases. Similarly, for samples obtained from zinc chloride and zinc nitrate, the texture coefficient increases with increasing solution concentration up to 0.2 M. However, for them, beyond 0.2 M, the $T_{C(hkl)}$ values decrease, revealing a random growth of crystallites. The obtained $T_{C(hkl)}$ values of each sample are in good agreement with the XRD patterns. It is worth mentioning that, the increase in $T_{C(hkl)}$ values indicates good crystallinity but this leads to an increase in grain boundary imbalance and introduces additional porosity into the thin film (Soylu *et al.*, 2018).

The lattice parameters a and c, and the interplanar distance d_{hkl} of the hexagonal wurtzite structure of all the ZnO samples elaborated are calculated from the relationships (12-14) (Kherchachi *et al.*, 2016) and are shown in Tables 2.

$$a^2 = \frac{\lambda^2(A_1B_2 - A_2B_1)}{3(B_2\sin^2\theta_1 - B_1\sin^2\theta_2)} \tag{12}$$

$$c^2 = \frac{\lambda^2(A_1B_2 - A_2B_1)}{4(A_1\sin^2\theta_2 - A_2\sin^2\theta_1)} \tag{13}$$

Table 2
Lattice parameters and structural properties of ZnO nanostructures obtained along the (002) plane with different precursor concentrations for (a) zinc acetate, (b) zinc chloride and (c) zinc nitrate

a) zinc acetate										
Precursors concentration	$2\theta(°)$	FWHM (°)	D(nm)	d(Å)	δ (x10^{14}lines $/m^2$)	Lattice parameters			L(Å)	V(Å^3)
						a (Å)	c(Å)	c /a		
0.1M	34.364	0.229	36.201	2.611	7.631	3.259	5.210	1.598	1.982	47.927
0.2M	34.310	0.194	42.687	2.612	5.488	3.266	5.213	1.596	1.984	48.114
0.3M	34.364	0.204	40.628	2.612	6.056	3.267	5.199	1.591	1.984	48.062
JCPDS no. 36-1451	34.422	-	-	2.603	-	3.250	5.207	1.602	-	47.622

b) zinc chloride										
Precursors concentration	$2\theta(°)$	FWHM (°)	D(nm)	d(Å)	δ (x10^{14}lines $/m^3$)	Lattice parameters			L(Å)	V(Å^3)
						a (Å)	c(Å)	c / a		
0.1M	34.364	0.183	45.484	2,608	4.834	3.259	5.210	1.596	1.982	47.927
0.2M	34.310	0.186	44.590	2.612	5.029	3.259	5.210	1.596	1.982	47.927
0.3M	34.416	0.195	42.709	2.608	5.482	3.254	5.210	1.601	1.982	47.927
JCPDS no. 36-1451	34.422	-	-	2.603	-	3.250	5.207	1.602	-	47.622

c) zinc nitrate										
Precursors concentration	$2\theta(°)$	FWHM (°)	D(nm)	d(Å)	δ (x10^{14} lines$/m^2$)	Lattice parameters			L(Å)	V(Å^3)
						a (Å)	c(Å)	c / a		
0.1M	34.310	0.279	29.749	2.612	0.112	3.262	5.197	1.593	1.982	47.876
0.2M	34.310	0.256	32.477	2.612	9.480	3.265	5.213	1.596	1.985	48.114
0.3M	34.310	0.247	33.661	2.612	8.825	3.265	5.213	1.596	1.985	48.114
JCPDS no. 36-1451	34.422	-	-	2.603	-	3.250	5.207	1.602	-	47.622

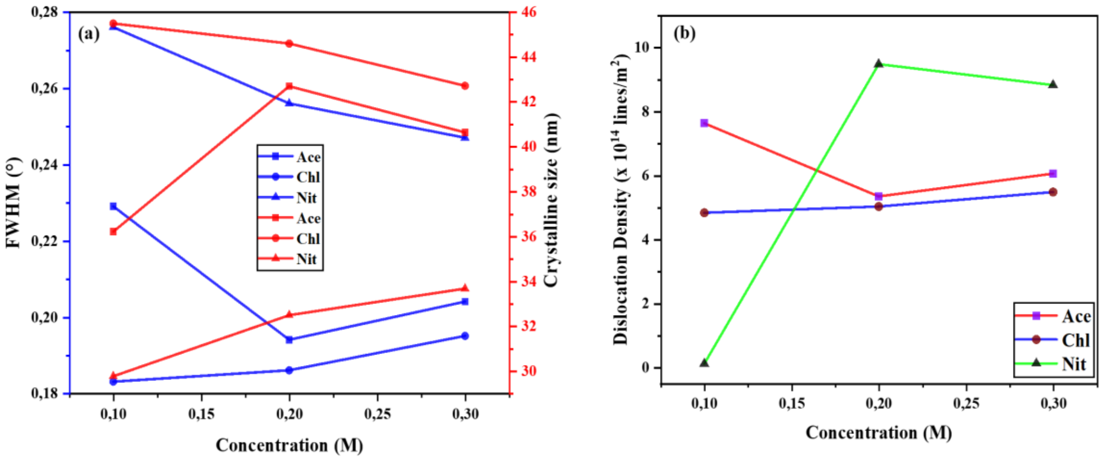

Fig. 2. Effect of different concentrations on the ZnO thin films (a) FWHM and crystalline sizes, (b) dislocation density

$$\frac{1}{{d_{hkl}}^2} = \frac{4}{3}\left(\frac{h^2 + hk + k^2}{a^2}\right) + \frac{l^2}{c^2} \tag{14}$$

where λ is wavelength of X-rays (1.540Å), θ is the diffraction angle, h,k,l are the Miller indices, d_{hkl} is the interplanar distance, coefficients. A_1, A_2, B_1 and B_2 are determined for a pair of planes $(h_1 k_1 k_1)$ and $(h_2 k_2 l_2)$ corresponding respectively to angles θ_1 and θ_2 such that:

$$\begin{cases} A_1 = h_1^2 + h_1 k_1 + k_1^2 \\ A_2 = h_2^2 + h_2 k_2 + k_2^2 \end{cases} ; \quad \begin{cases} B_1 = l_1^2 \\ B_2 = l_2^2 \end{cases} .$$

As it can be seen in Table 2, the calculated parameters a and c are roughly equal to the standard reference values (a = 3.249 Å and c = 5.206 Å) in JCPDS file no. 36-1451. No significant change in the parameters values is observed either for precursor sources nor for solution concentration. The c/a ratio value of ≃ 1.60 obtained for all the samples indicates that all the deposited ZnO thin films have a well compacted hexagonal structure. No variation of the d_{hkl} value is observed for zinc acetate and zinc nitrate regardless of the solution concentration. The slight change observed for zinc chloride can be attributed to atom position shifting (Bindu *et al.*, 2014).

The influence of precursor concentration on crystallite size (Fig. 2a), bond length (Fig. 2b), cell volume (Fig. 2c) and dislocation density (Fig. 2d) has been studied. The crystallite size (D) was calculated using the Debye Scherrer formula (eq.15) (Gaikwad *et al.*, 2014) :

$$D = \frac{k\lambda}{\beta cos\theta} \tag{15}$$

where k is a constant which is taken to be 0.9, λ the wavelength of the source considered, β the full width at half maximum of the peak (FWHM) and θ the Bragg diffraction angle.

The dislocation density (δ), which represents the number of defects arising from internal deformation and the offset between substrate and crystal growth, was calculated according to equation (AL-Arique *et al.*, 2024) (16):

$$\delta = \frac{1}{D^2} \tag{16}$$

where D is the crystallite size.
The volume of the hexagonal cell (v) was evaluated using equation (17):

$$v = \left(\frac{\sqrt{3}}{2}\right) a^2 c \tag{17}$$

where a and c are the lattice parameters.
The bond length of ZnO was calculated from equation (18) (Abbas *et al.,* 2024):

$$L = \sqrt{\frac{a^2}{3} + \left(\frac{1}{2} - u\right)^2 . c^2} \tag{18}$$

where u, a parameter related to the c/a ratio, is a measurement of the amount each atom is displaced with respect to the next one along the c-axis, and is given by equation (19) (Amroun *et al.*, 2020)

$$u = \frac{a^2}{3c^2} + 0.25 \tag{19}$$

It can be seen from Fig. 2a that, for the sample obtained from zinc nitrate, the crystallite size increases from 29.749 nm to 33.661 nm with increase in precursor concentration. In the case of zinc chloride, we observed the opposite behavior: crystallite size decreases from 45.484 nm to 42.709 nm with increase in precursor concentration. For zinc acetate, crystallite size increases from 36.201 nm to 42.687 nm with increasing precursor concentration up to 0.2 M and then decreases to 40.628 nm with further increase in precursor concentration. From these results, we conclude that, for zinc nitrate, high concentration leads to large crystallite size while for zinc chloride, high concentration leads to small crystallite size. With zinc acetate, ZnO crystallite size is not linear to precursor concentration. In our case, the saturation is reached at 0.2 M precursor concentration and as a consequence we observed the decrease in crystallite size.

Fig. 2b shows the dislocation density of the elaborated ZnO thin films. It can be seen that, for films obtained from zinc chloride, dislocation density increases with increasing precursor concentration. In the case of samples elaborated from zinc nitrate, the dislocation density increases with increase in precursor concentration up to 0.2 M and then decreases with further increase. On other hand, for samples elaborated from zinc acetate the dislocation density decreases with increase in precursor concentration up to 0.2 M then increases with further increase in precursor concentration. It should be mentioned that the variations observed in dislocation density values can be

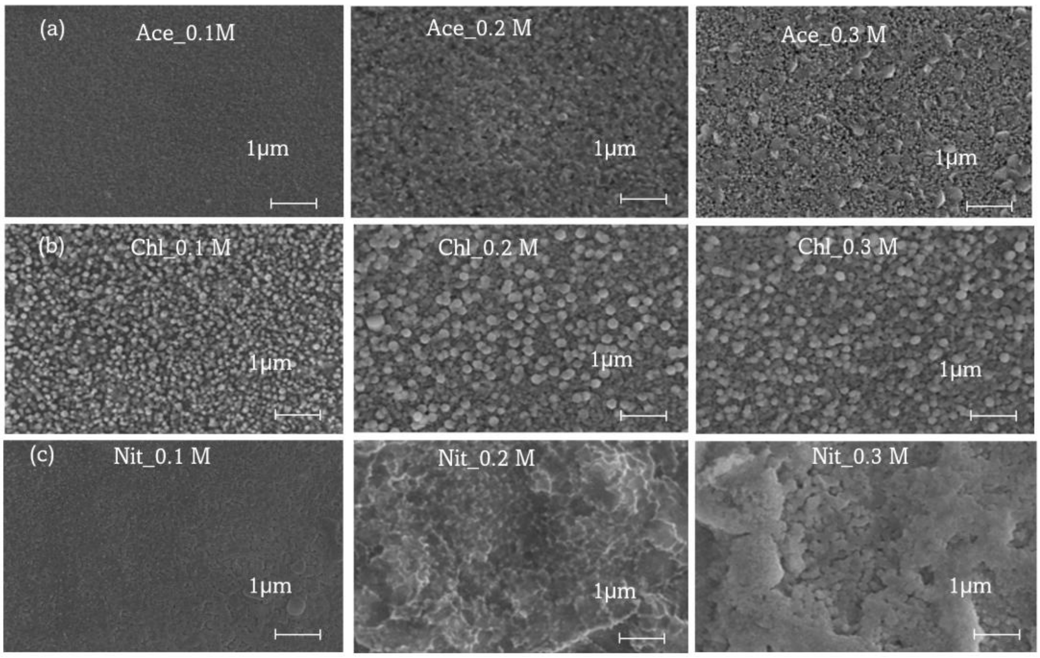

Fig. 3. SEM images of ZnO thin films for (a) zinc acetate, (b) zinc chloride and (c) zinc nitrate

attributed to the film growth mechanisms. The growth mechanism that occurs using zinc chloride may be related to Stranski-Krastanov growth (Kaiser, 2002). This mechanism involves an initial layer-by-layer growth followed by island formation. The transition from layer growth to islanding can lead to increased misfit dislocations due to lattice mismatch between the film and substrate. As the film thickness increases beyond a critical point, both misfit and threading dislocations are generated, significantly raising the dislocation density. Using zinc acetate and zinc nitrate, the growth mechanism may be related to Volmer-Weber growth (Kaiser, 2002). It leads to three-dimensional island formation from the onset. This mechanism tends to produce higher dislocation densities compared to layer-by-layer mechanism because islands can coalesce, resulting in increased strain and subsequent dislocation generation.

3.2 Morphological properties

Surface morphology of ZnO samples deposited at growth temperature of 350°C with different molarities and different zinc precursors are presented in Fig. 3. As can be seen, the film's morphology depends strongly on the nature of the precursors. Films obtained from zinc nitrate (Fig. 3c) looked dense and compact while zinc chloride (Fig. 3b) and zinc acetate (Fig. 3a) gave uniform and homogeneous films with well-formed and distinguished grains. Regardless of the source of the precursor, it can be observed that grain size increases as concentration of precursors increases. We note that zinc chloride film exhibited highest grain size.

The difference in morphology is induced by the growth mechanism, since all the precursors don't have the same properties (surface tension, viscosity) (Al-Rasheedi *et al.*, 2022b). It is well known that, using spray pyrolysis technique, film formation passes three steps (Znaidi *et al.*, 2003): (i) solution atomization to generate droplet's (ii) droplets spraying on heated surface (iii) surface reaction. By spraying the solution on the substrate, the droplet's dynamics is controlled by the solution properties. Hence, each step may have an influence on the film deposited. It is reported that among the three precursors, zinc chloride has the largest surface tension and viscosity (Bacaksiz *et al.*, 2008). So, the incoming droplets cannot easily move on the substrate surface. As a consequence, the ZnO film grows along the c axis with a large spherical grain shape (Fig. 3b). By increasing precursor concentration up to 0.2 M, film starts to grow randomly leading to increased roughness in film surface. This is consistent with the XRD results. The same trend is observed for zinc acetate film.

However, in the case of zinc acetate small grains are formed leading to a smooth and uniform film surface (Fig. 3a) aggregated at high (0.3 M) precursor molarity (Fig. 3a). As the zinc nitrate has low surface tension and viscosity, the droplets easily spread on the substrate limiting vertical film growth. Moreover, as zinc nitrate atoms present more affinity when increasing precursor concentration, highly compact and rough films are formed (Fig. 3c).

Overall, it can be seen that ZnO films from zinc acetate and nitrate exhibit smoother surfaces compared to zinc chloride because they tend to form more uniform and stable sols, which lead to smoother film surfaces. In particular, zinc acetate is known for producing ZnO nanoparticles with reduced crystalline size and high surface area, which can contribute to smoother films (Gatou *et al.*, 2023). Moreover, zinc chloride often gives rise to ZnO rods or microrods, which can lead to a more textured surface morphology. The rod-like structures can increase the surface roughness compared to films derived from acetate or nitrate precursors (Bacaksiz *et al.*, 2008)

3.3 Optical properties

Fig. 4 shows the optical spectra of ZnO thin films deposited from different precursors: zinc acetate (Fig. 4a), zinc chloride (Fig. 4b) and zinc nitrate (Fig. 4c) with varied precursor concentrations. The optical transmission was measured in the 380 to 800nm wavelength range. As it can be seen, the film transmittance strongly depends on the used precursor and precursor concentration: zinc acetate (80-95%), zinc chloride (50-94%) and zinc nitrate (35-65%).

The difference observed in film transmittance is related to surface morphology and grain size. The films deposited from zinc acetate exhibit the highest transmittance (Fig. 4a). This can

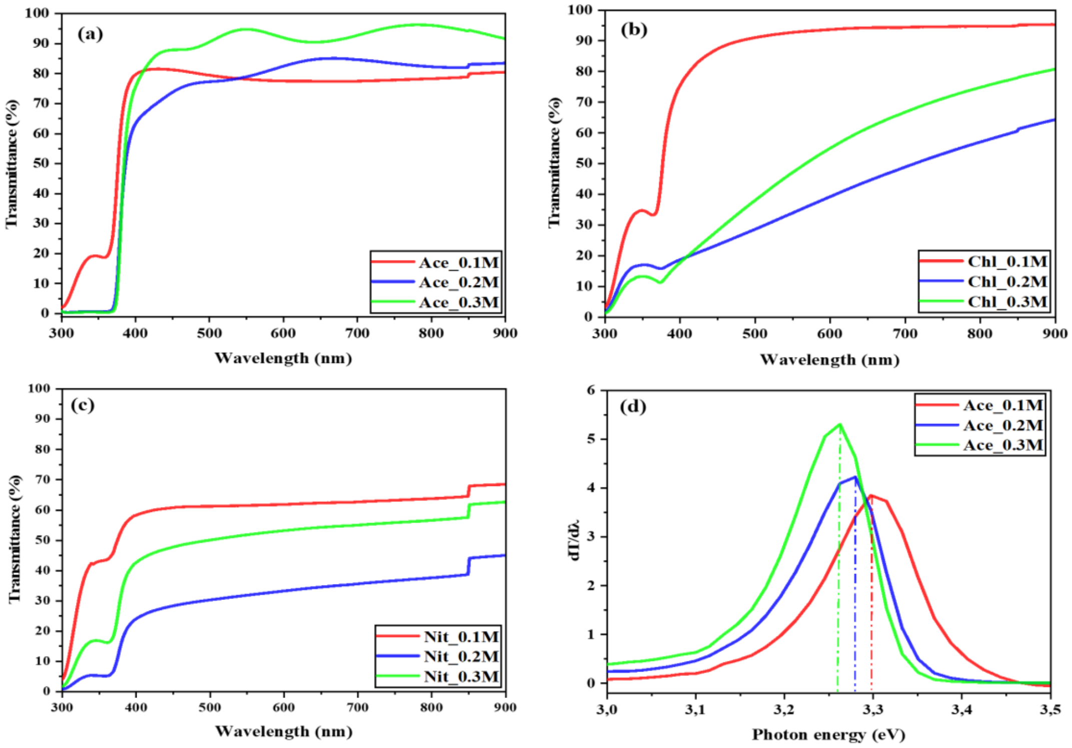

Fig. 4. Optical transmissions spectra of ZnO thin films for (a) zinc acetate, (b) zinc chloride and (c) zinc nitrate precursors, and (d) the band gaps of ZnO prepared with zinc acetate precursor

be explained by the fact that Zinc acetate films have smooth and uniform film surfaces. Moreover, it is observed that transmittance increases with increase in precursor concentration. This can be due in the case of zinc acetate, to film crystallinity increases with increasing precursor concentration as shown in XRD results. Zinc chloride films exhibit high transmittance for films deposited from 0.1 M solution. By increasing precursor concentration, transmittance decreases drastically (Fig. 4b). This can be explained by the formation of large grains which increase surface roughness. It is well known that rough surfaces cause light scattering to reduce the films' transmittance. For zinc nitrate, although films exhibit good crystallinity, the transmittance is the lowest compared to the other precursors. The low transmittance observed for zinc nitrate (Fig. 4c) films is due to the highly compact and rough surface morphology.

Among the three precursors studied, zinc acetate exhibits the best morphological and optical properties. The band gap of the samples prepared with zinc acetate was determined by calculating the derivative of the transmittance with respect to the light wavelength ($dT/d\lambda$) and plotting the ($dT/d\lambda$) curve as a function of photon energy (Xu *et al.*, 2020), as shown in Fig. 4d. The band gap of ZnO obtained from the zinc acetate precursor decreases with increasing solution concentration. It is found to be 3.29 eV, 3.26 eV, and 3.22 eV for concentrations of 0.1M, 0.2M, and 0.3M, respectively. The decrease in the band gap of ZnO thin films with increasing precursor concentration can be attributed to several factors related to the structural and optical properties of the films: i) Higher precursor concentrations often lead to thicker films with larger grain sizes or more defects. Larger grains can reduce the band gap due to the decrease in quantum confinement effects, which typically increase the band gap in smaller grains. In addition, increased defects can introduce mid-gap states which can lead to reduced band gap by providing additional paths for electron transitions (Nagayasamy *et al.*, 2013). ii) Higher precursor concentrations can result in films with increased strain due to differences in thermal expansion between the film and the substrate. Strain can alter the band structure, potentially reducing the band gap (Rama Denny *et al.*, 2020). iii) Higher precursor concentrations can lead to larger grain size, which might enhance optical scattering and affect the measured band gap. (Amananti *et al.*, 2022)

3.4 FTIR analysis

In order to identify the functional groups, present in ZnO elaborated films, all the samples were characterized by FTIR spectroscopy within the range of 4000 - 400 cm^{-1} using Gladi-ATR (Attenuated Total Reflectance) method. Fig. 5 shows the FTIR spectra of ZnO thin films grown using zinc acetate (Fig. 5a), zinc chloride (Fig. 5b) and zinc nitrate (Fig. 5c) as precursors.

All the samples exhibit almost the same absorption peaks. The peaks observed between 2850 cm^{-1} and 2930 cm^{-1}, correspond to the C-H stretching vibration of alkane groups (Gopikrishnan *et al.*, 2010), which may come from the precursors used. The peaks observed around 2150 cm^{-1} are associated with the O=C=O stretching mode of carbon dioxide (Gatou *et al.*, 2023). An absorption peak is also observed at 1590 cm^{-1}, attributed to the symmetric C=O stretching (Ibrahim *et al.*, 2018). The peaks located between 700 cm^{-1} and 1200 cm^{-1} are related to the H-O-H bending vibration, due to the presence of crystallization water from the solvent used (D. Yu *et al.*, 2015). The peak observed at 883 cm^{-1} is also attributed to the deformation vibration of water molecules. For the sample obtained with zinc nitrate, a strong absorption peak at 883 cm^{-1} is observed, which intensity decreases until it completely disappears as the concentration increases. O-H vibration peaks observed between 3500 cm^{-1} and 4000 cm^{-1}, for samples

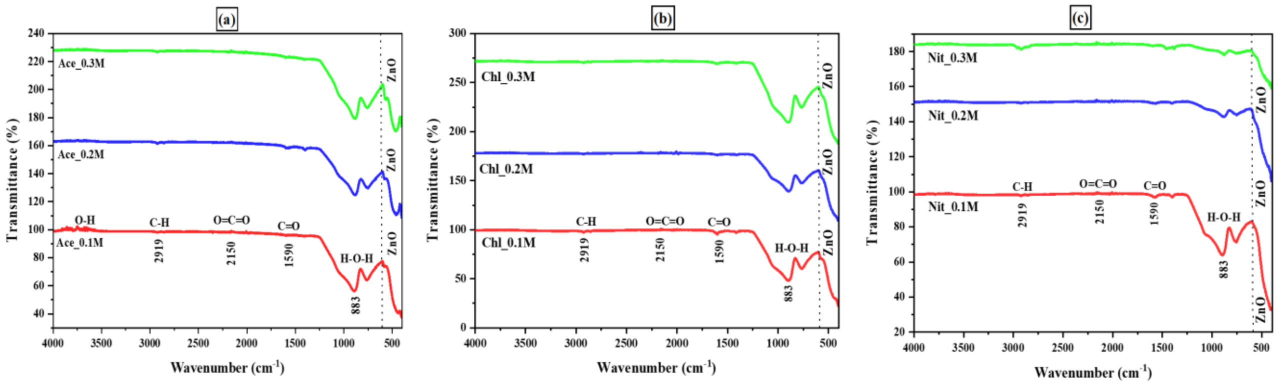

Fig 5. The FTIR spectra of ZnO thin films for (a) zinc acetate, (b) zinc chloride and (c) zinc nitrate precursors

obtained from zinc acetate may be originated from ethanol used as solvent (Bulcha *et al.*, 2021). Finally, the band between 400 cm^{-1} and 600 cm^{-1}, present in all samples, corresponds to the Zn-O vibration, as confirmed by previous studies (Abdelghani *et al.*, 2022).

4. Conclusion

ZnO thin films were prepared using zinc acetate, zinc chloride and zinc nitrate precursors by spray pyrolysis methods on glass substrates at 350°C and annealed at 400°C for 3 hours. The effects of different precursors with different concentrations have been studied. The concentration of each precursor varied from 0.1 M to 0.3 M. The results of the XRD characterization show that whatever the precursor used, the ZnO thin films are polycrystalline and crystallize in the hexagonal wurtzite structure. The films obtained from the zinc acetate and zinc nitrate precursors show a preferential orientation along (002) as the concentration increases, while the film obtained from zinc chloride shows a random orientation beyond 0.2 M. SEM images show that surface morphology strongly depends on the source of the precursor. The UV-visible spectrophotometer analysis indicated that ZnO films obtained from zinc chloride precursors with 0.1M concentration are highly transparent (94 %) in the visible region. However, films' transmittance decreases drastically (50 %) by increasing precursor concentration. The transmittance value was 80 – 95 % for the zinc acetate precursor with a maximum value of 95 % obtained for the concentration of 0.3 M. The ZnO films elaborated from zinc nitrate exhibited the lowest optical transmittance (35 – 65 %). ZnO films obtained from zinc acetate are more suitable for photovoltaic applications as they exhibit the best crystallinity and the highest transmittance.

Acknowledgements

The authors would like to thank the Indian government, Department of Nano Science and Technology; Karunya University, through CV Raman International Fellowship program for African Researchers.

References

Abbas, F. I., & Sugiyama, M. (2024). Solution-dependent electrostatic spray deposition (ESD) ZnO thin film growth processes. *Materials Science*. https://doi.org/10.48550/arXiv.2406.13313

Abdelghani, G. M., Ahmed, A. B., & Al-Zubaidi, A. B. (2022). Synthesis, characterization, and the influence of energy of irradiation on optical properties of ZnO nanostructures. *Scientific Reports*, *12*(1), 20016. https://doi.org/10.1038/s41598-022-24648-x

Abdulrazzaq, O. A., Saini, V., Bourdo, S., Dervishi, E., & Biris, A. S. (2013). Organic Solar Cells: A Review of Materials, Limitations, and Possibilities for Improvement. *Particulate Science and Technology*, *31*(5), 427–442. https://doi.org/10.1080/02726351.2013.769470

Akir, S., Hamdi, A., Addad, A., Coffinier, Y., Boukherroub, R., & Dakhlaoui Omrani, A. (2017). Facile synthesis of carbon-ZnO nanocomposite with enhanced visible light photocatalytic performance. *Applied Surface Science*, *400*, 461–470. https://doi.org/10.1016/j.apsusc.2016.12.212

AL-Arique, H. Q. N. M., AL-Qadasy, S. S. S., Kaawash, N. M. S., Chishty, S. Q., & Bogle, K. A. (2024). Study the characterization of ZnO and AZO films prepared by spray pyrolysis and the effect of annealing temperature. *Optical Materials*, *150*, 115261. https://doi.org/10.1016/j.optmat.2024.115261

Al-Rasheedi, A., Ansari, A. R., Abdeldaim, A. M., & Aida, M. S. (2022a). Growth of zinc oxide thin films using different precursor solutions by spray pyrolysis technique. *The European Physical Journal Plus*, *137*(12), 1371. https://doi.org/10.1140/epjp/s13360-022-03599-2

Al-Rasheedi, A., Ansari, A. R., Abdeldaim, A. M., & Aida, M. S. (2022b). Growth of zinc oxide thin films using different precursor solutions by spray pyrolysis technique. *The European Physical Journal Plus*, *137*(12), 1371. https://doi.org/10.1140/epjp/s13360-022-03599-2

Amananti, W., Ardiyanto, R., Sutanto, H., Nurhasanah, I., & Tivani, I. (2022). Analysis of the optical properties of ZnO thin films deposited on a glass substrate by the So-gel method. *Journal of Natural Sciences and Mathematics Research*, *8*(1), 52–58. https://doi.org/10.21580/jnsmr.2022.8.1.9623

Amroun, M. N., Salim, K., Kacha, A. H., & Khadraoui, M. (2020). Effect of TM (TM= Sn, Mn, Al) Doping on the Physical Properties of ZnO Thin Films Grown by Spray Pyrolysis Technique: A comparative Study. *International Journal of Thin Films Science and Technology*, *9*(1), 7–19. https://doi.org/10.18576/ijtfst/090102

Arca, E., Fleischer, K., & Shvets, I. V. (2009). Influence of the Precursors and Chemical Composition of the Solution on the Properties of ZnO Thin Films Grown by Spray Pyrolysis. *The Journal of Physical Chemistry C*, *113*(50), 21074–21081. https://doi.org/10.1021/jp907990z

Arifin, N. M., Mhd Noor, E. E., Mohamad, F., & Mohamad, N. (2024). The Impact of Spinning Speed on n-TiO2/ZnO Bilayer Thin Film Fabricated through Sol–Gel Spin-Coating Method. *Coatings*, *14*(1), 73. https://doi.org/10.3390/coatings14010073

Bacaksiz, E., Parlak, M., Tomakin, M., Özçelik, A., Karakız, M., & Altunbaş, M. (2008). The effects of zinc nitrate, zinc acetate and zinc chloride precursors on investigation of structural and optical properties of ZnO thin films. *Journal of Alloys and Compounds*, *466*(1–2), 447–450. https://doi.org/10.1016/j.jallcom.2007.11.061

Balderrama, V. S., Sánchez, J. G., Lastra, G., Cambarau, W., Arias, S., Pallarès, J., Palomares, E., Estrada, M., & Marsal, L. F. (2018). High-efficiency organic solar cells based on a halide salt and polyfluorene polymer with a high alignment-level of the cathode selective contact. *Journal of Materials Chemistry A*, *6*(45), 22534–22544. https://doi.org/10.1039/C8TA05778H

Bindu, P., & Thomas, S. (2014). Estimation of lattice strain in ZnO nanoparticles: X-ray peak profile analysis. *Journal of Theoretical and Applied Physics*, *8*(4), 123–134. https://doi.org/10.1007/s40094-014-0141-9

Bulcha, B., Leta Tesfaye, J., Anatol, D., Shanmugam, R., Dwarampudi, L. P., Nagaprasad, N., Bhargavi, V. L. N., & Krishnaraj, R. (2021). Synthesis of Zinc Oxide Nanoparticles by Hydrothermal Methods and Spectroscopic Investigation of Ultraviolet Radiation Protective Properties. *Journal of Nanomaterials*, *2021*, 1–10. https://doi.org/10.1155/2021/8617290

Chen, H., Hu, D., Yang, Q., Gao, J., Fu, J., Yang, K., He, H., Chen, S., Kan, Z., Duan, T., Yang, C., Ouyang, J., Xiao, Z., Sun, K., & Lu, S. (2019). All-Small-Molecule Organic Solar Cells with an Ordered Liquid Crystalline Donor. *Joule*, *3*(12), 3034–3047. https://doi.org/10.1016/j.joule.2019.09.009

Chen, J., Cui, C., Li, Y., Zhou, L., Ou, Q., Li, C., Li, Y., & Tang, J. (2015). Single-Junction Polymer Solar Cells Exceeding 10% Power Conversion Efficiency. *Advanced Materials*, *27*(6), 1035–1041. https://doi.org/10.1002/adma.201404535

Cho, J., Hwang, S., Ko, D.-H., & Chung, S. (2019). Transparent ZnO Thin-Film Deposition by Spray Pyrolysis for High-Performance Metal-Oxide Field-Effect Transistors. *Materials*, *12*(20), 3423. https://doi.org/10.3390/ma12203423

Dakhsi, K., Hartiti, B., Elfarrass, S., Tchognia, H., & Touhami, M. E. (2014). Étude des propriétés structurales, optiques et électriques des couches minces de ZnO dopées Al déposées par Spray Pyrolysis. *Afrique SCIENCE*.

De Jong, M. P., Van IJzendoorn, L. J., & De Voigt, M. J. A. (2000). Stability of the interface between indium-tin-oxide and poly(3,4-ethylenedioxythiophene)/poly(styrenesulfonate) in polymer light-emitting diodes. *Applied Physics Letters*, *77*(14), 2255–2257. https://doi.org/10.1063/1.1315344

Ekmekci, M., Ela, C., & Erten-Ela, S. (2019). Morphological characterization of aluminum-doped zinc oxide nanomaterials (AZO) for dye-sensitized solar cells. *International Journal of Applied Ceramic Technology*, *16*(2), 727–734. https://doi.org/10.1111/ijac.13113

Foo, K. L., Hashim, U., Muhammad, K., & Voon, C. H. (2014). Sol–gel synthesized zinc oxide nanorods and their structural and optical investigation for optoelectronic application. *Nanoscale Research Letters*, *9*(1), 429. https://doi.org/10.1186/1556-276X-9-429

Fu, H., Li, Y., Yu, J., Wu, Z., Fan, Q., Lin, F., Woo, H. Y., Gao, F., Zhu, Z., & Jen, A. K.-Y. (2021). High Efficiency (15.8%) All-Polymer Solar Cells Enabled by a Regioregular Narrow Bandgap Polymer Acceptor. *Journal of the American Chemical Society*, *143*(7), 2665–2670. https://doi.org/10.1021/jacs.0c12527

Gaikwad, R. S., Jagdale, S. B., Pol, P. B., Mohite, K. C., & Pawar, B. N. (2014). Effect of Concentration of Precursor on Intrinsic ZnO Thin Films by Spray Pyrolysis. *Asian Journal of Multidisciplinary Studies*, 2(5)

Gatou, M.-A., Lagopati, N., Vagena, I.-A., Gazouli, M., & Pavlatou, E. A. (2023). ZnO Nanoparticles from Different Precursors and Their Photocatalytic Potential for Biomedical Use. *nanomaterials*, *13*(122). https:/ /doi.org/10.3390/ nano13010122

Gopikrishnan, R., Zhang, K., Ravichandran, P., Baluchamy, S., Ramesh, V., Biradar, S., Ramesh, P., Pradhan, J., Hall, J. C., Pradhan, A. K., & Ramesh, G. T. (2010). Synthesis, characterization and biocompatibility studies of zinc oxide (ZnO) nanorods for biomedical application. *Nano-Micro Letters*, *2*(1), 31–36. https://doi.org/10.1007/BF03353614

Halls, J. J. M., Walsh, C. A., Greenham, N. C., Marseglia, E. A., Friend, R. H., Moratti, S. C., & Holmes, A. B. (1995). Efficient photodiodes from interpenetrating polymer networks. *Letters to Nature*.

Hatem, D., Nemmar, F., & Belkaid, M. S. (2023). Cellules solaires organiques: choix des matériaux, structures des dispositifs et amélioration du rendement et de la stabilité. *Journal of Renewable Energies*, *12*(1). https://doi.org/10.54966/jreen.v12i1.121

He, Z., Xiao, B., Liu, F., Wu, H., Yang, Y., Xiao, S., Wang, C., Russell, T. P., & Cao, Y. (2015). Single-junction polymer solar cells with high efficiency and photovoltage. *Nature Photonics*, *9*(3), 174–179. https://doi.org/10.1038/nphoton.2015.6

He, Z., Zhong, C., Su, S., Xu, M., Wu, H., & Cao, Y. (2012). Enhanced power-conversion efficiency in polymer solar cells using an inverted device structure. *Nature Photonics*, *6*(9), 591–595. https://doi.org/10.1038/nphoton.2012.190

Ibrahim, N. A., Nada, A. A., Eid, B. M., Al-Moghazy, M., Hassabo, A. G., & Abou-Zeid, N. Y. (2018). Nano-structured metal oxides: synthesis, characterization and application for multifunctional cotton fabric. *Advances in Natural Sciences: Nanoscience and Nanotechnology*, *9*(3), 035014. https://doi.org/10.1088/2043-6254/aadc2c

Irish, D. E., McCarroll, B., & Young, T. F. (1963). Raman Study of Zinc Chloride Solutions. *The Journal of Chemical Physics*, *39*(12), 3436–3444. https://doi.org/10.1063/1.1734212

Jørgensen, M., Norrman, K., & Krebs, F. C. (2008). Stability/degradation of polymer solar cells. *Solar Energy Materials and Solar Cells*, *92*(7), 686–714. https://doi.org/10.1016/j.solmat.2008.01.005

Kaiser, N. (2002). Review of the fundamentals of thin-film growth. *Applied Optics*, *41*(16), 3053. https://doi.org/10.1364/AO.41.003053

Kärber, E., Raadik, T., Dedova, T., Krustok, J., Mere, A., Mikli, V., & Krunks, M. (2011). Photoluminescence of spray pyrolysis deposited ZnO nanorods. *Nanoscale Research Letters*, *6*(1), 359. https://doi.org/10.1186/1556-276X-6-359

Kherchachi, I. B., Saidi, H., Attaf, A., Attaf, N., Bouhdjar, A., Bendjdidi, H., Benkhetta, Y., Azizi, R., & Jlassi, M. (2016). Influence of solution flow rate on the properties of SnS2 films prepared by ultrasonic spray. *Optik*, *127*(8), 4043–4046. https://doi.org/10.1016/j.ijleo.2016.01.120

Kozawa, T., Onda, A., Yanagisawa, K., Kishi, A., & Masuda, Y. (2011). Effect of water vapor on the thermal decomposition process of zinc hydroxide chloride and crystal growth of zinc oxide. *Journal of Solid State Chemistry*, *184*(3), 589–596. https://doi.org/10.1016/j.jssc.2011.01.015

Krebs, F. C. (2009). Fabrication and processing of polymer solar cells: A review of printing and coating techniques. *Solar Energy Materials and Solar Cells*, *93*(4), 394–412. https://doi.org/10.1016/j.solmat.2008.10.004

Krebs, F. C., & Norrman, K. (2007). Analysis of the failure mechanism for a stable organic photovoltaic during 10 000 h of testing. *Progress in Photovoltaics: Research and Applications*, *15*(8), 697–712. https://doi.org/10.1002/pip.794

Li, G., Zhu, R., & Yang, Y. (2012). Polymer solar cells. *Nature Photonics*, *6*(3), 153–161. https://doi.org/10.1038/nphoton.2012.11

Li, T., Chen, Z., Wang, Y., Tu, J., Deng, X., Li, Q., & Li, Z. (2020). Materials for Interfaces in Organic Solar Cells and Photodetectors. *ACS Applied Materials & Interfaces*, *12*(3), 3301–3326. https://doi.org/10.1021/acsami.9b19830

Lin, C.-C., & Li, Y.-Y. (2009). Synthesis of ZnO nanowires by thermal decomposition of zinc acetate dihydrate. *Materials Chemistry and Physics*, *113*(1), 334–337. https://doi.org/10.1016/j.matchemphys.2008.07.070

Lin, Y., Adilbekova, B., Firdaus, Y., Yengel, E., Faber, H., Sajjad, M., Zheng, X., Yarali, E., Seitkhan, A., Bakr, O. M., El-Labban, A., Schwingenschlögl, U., Tung, V., McCulloch, I., Laquai, F., & Anthopoulos, T. D. (2019). 17% Efficient Organic Solar Cells Based on Liquid Exfoliated WS_2 as a Replacement for PEDOT:PSS. *Advanced Materials*, *31*(46), 1902965. https://doi.org/10.1002/adma.201902965

Maneva, M., & Petrov, N. (1989). on the thermal decomposition of Zn(NO3)2.6H2O and its deuterated analogue. *Journal of Thermal Analysis*, *35*.

Mani, G. K., & Rayappan, J. B. B. (2014). Novel and facile synthesis of randomly interconnected ZnO nanoplatelets using spray pyrolysis and their room temperature sensing characteristics. *Sensors and Actuators B: Chemical*, *198*, 125–133. https://doi.org/10.1016/j.snb.2014.02.101

Mishra, M., Banga, V. P., Kumar, M., & Gupta, M. (2024). Effect of aging on transmittance, and effect of annealing temperature on CO2 sensing of ZnO thin film deposited by spin coating. *E-Prime - Advances in Electrical Engineering, Electronics and Energy*, *7*, 100405. https://doi.org/10.1016/j.prime.2023.100405

Morinaga, Y., Sakuragi, K., Fujimura, N., & Ito, T. (1997). Effect of Ce doping on the growth of ZnO thin films. *Journal of Crystal Growth*, *174*(1–4), 691–695. https://doi.org/10.1016/S0022-0248(97)00045-6

Moustafa, E., Sánchez, J. G., Marsal, L. F., & Pallarès, J. (2021). Stability Enhancement of High-Performance Inverted Polymer Solar Cells Using ZnO Electron Interfacial Layer Deposited by Intermittent

Spray Pyrolysis Approach. *ACS Applied Energy Materials*, *4*(4), 4099–4111. https://doi.org/10.1021/acsaem.1c00455

Nagayasamy, N., Gandhimathination, S., & Veerasamy, V. (2013). The Effect of ZnO Thin Film and Its Structural and Optical Properties Prepared by Sol-Gel Spin Coating Method. *Open Journal of Metal*, *03*(02), 8–11. https://doi.org/10.4236/ojmetal.2013.32A2002

Osorio, E., Sánchez, J. G., Acquaroli, L. N., Pacio, M., Ferré-Borrull, J., Pallarès, J., & Marsal, L. F. (2017). Degradation Analysis of Encapsulated and Nonencapsulated TiO_2 /PTB7:PC_{70} BM/V_2 O_5 Solar Cells under Ambient Conditions via Impedance Spectroscopy. *ACS Omega*, *2*(7), 3091–3097. https://doi.org/10.1021/acsomega.7b00534

Podlogar, M., Richardson, J. J., Vengust, D., Daneu, N., Samardžija, Z., Bernik, S., & Rečnik, A. (2012). Growth of Transparent and Conductive Polycrystalline (0001)-ZnO Films on Glass Substrates Under Low-Temperature Hydrothermal Conditions. *Advanced Functional Materials*, *22*(15), 3136–3145. https://doi.org/10.1002/adfm.201200214

Rama Denny, Y., Firmansyah, T., Trenggono, A., Wijaya, D., Antarnusa, G., & Suherman, A. (2020). Effect of Precursor Concentration and Annealed Substrate Temperature on the Crystal Structure, Electronic and Optical Properties of ZnO thin film. *The Journal of Pure and Applied Chemistry Research*, *9*(1), 57–65. https://doi.org/10.21776/ub.jpacr.2020.009.01.514

Ravichandran, K., Jabena Begum, N., Snega, S., & Sakthivel, B. (2016). Properties of Sprayed Aluminum-Doped Zinc Oxide Films—A Review. *Materials and Manufacturing Processes*, *31*(11), 1411–1423. https://doi.org/10.1080/10426914.2014.930961

Salsberg, E., & Aziz, H. (2019). Degradation of PEDOT:PSS hole injection layers by electrons in organic light emitting devices. *Organic Electronics*, *69*, 313–319. https://doi.org/10.1016/j.orgel.2019.03.009

Shrisha, B. V., Bhat, S., Kushavah, D., & Gopalakrishna Naik, K. (2016). Hydrothermal growth and characterization of Al-doped ZnO nanorods. *Materials Today: Proceedings*, *3*(6), 1693–1701. https://doi.org/10.1016/j.matpr.2016.04.061

Soylu, M., & Coskun, M. (2018). Controlling the properties of ZnO thin films by varying precursor concentration. *Journal of Alloys and Compounds*, *741*, 957–968. https://doi.org/10.1016/j.jallcom.2018.01.079

Sun, C., Pan, F., Bin, H., Zhang, J., Xue, L., Qiu, B., Wei, Z., Zhang, Z.-G., & Li, Y. (2018). A low cost and high performance polymer donor material for polymer solar cells. *Nature Communications*, *9*(1), 743. https://doi.org/10.1038/s41467-018-03207-x

Thankalekshmi, R. R., & Rastogi, A. C. (2012). Structure and optical band gap of ZnO1−xSx thin films synthesized by chemical spray pyrolysis for application in solar cells. *Journal of Applied Physics*, *112*(6), 063708. https://doi.org/10.1063/1.4754014

Wong, K. W., Yip, H. L., Luo, Y., Wong, K. Y., Lau, W. M., Low, K. H., Chow, H. F., Gao, Z. Q., Yeung, W. L., & Chang, C. C. (2002). Blocking reactions between indium-tin oxide and poly (3,4-ethylene dioxythiophene):poly(styrene sulphonate) with a self-assembly monolayer. *Applied Physics Letters*, *80*(15), 2788–2790. https://doi.org/10.1063/1.1469220

Xu, L., Wang, X., Qian, L., Zhu, Y., Luo, X., Wang, W., Xu, X., & Xu, J. (2020). The dependence of the optical properties of ZnO nanorod arrays on their growth time. *Optik*, *202*, 163634. https://doi.org/10.1016/j.ijleo.2019.163634

Yu, D., Mu, S., Liu, L., & Wang, W. (2015). Preparation of electroless silver plating on aramid fiber with good conductivity and adhesion strength. *Colloids and Surfaces A: Physicochemical and Engineering Aspects*, *483*, 53–59. https://doi.org/10.1016/j.colsurfa.2015.07.021

Yu, G., Gao, J., Hummelen, J. C., Wudl, F., & Heeger, A. J. (1995). Polymer Photovoltaic Cells: Enhanced Efficiencies via a Network of Internal Donor-Acceptor Heterojunctions. *Science*, *270*(5243), 1789–1791. https://doi.org/10.1126/science.270.5243.1789

Zhang, D., Wu, X., Han, N., & Chen, Y. (2013). Chemical vapor deposition preparation of nanostructured ZnO particles and their gas-sensing properties. *Journal of Nanoparticle Research*, *15*(4), 1580. https://doi.org/10.1007/s11051-013-1580-y

Zhou, R., Jiang, Z., Yang, C., Yu, J., Feng, J., Adil, M. A., Deng, D., Zou, W., Zhang, J., Lu, K., Ma, W., Gao, F., & Wei, Z. (2019). All-small-molecule organic solar cells with over 14% efficiency by optimizing hierarchical morphologies. *Nature Communications*, *10*(1), 5393. https://doi.org/10.1038/s41467-019-13292-1

Znaidi, L., Soler Illia, G. J. A. A., Benyahia, S., Sanchez, C., & Kanaev, A. V. (2003). Oriented ZnO thin films synthesis by sol–gel process for laser application. *Thin Solid Films*, *428*(1–2), 257–262. https://doi.org/10.1016/S0040-6090(02)01219-1